CHEMICAL ENGINEERING TRANSACTIONS
VOL. 86, 2021
A publication of AIDIC
The Italian Association of Chemical Engineering
Online at www.cetjournal.it
Guest Editors: Sauro Pierucci, Jiří Jaromír Klemeš
Copyright © 2021, AIDIC Servizi S.r.l.
ISBN 978-88-95608-84-6; **ISSN** 2283-9216

Investigation of the fluid dynamic of the modified Hartmann tube equipment by high-speed video processing

Enrico Danzi[a], Fausto Franchini[a], Olivier Dufaud[b], Matteo Pietraccini[b] & Luca Marmo[a]

[a] Dipartimento di Scienza Applicata e Tecnologia-Politecnico di Torino, C.so Duca degli Abruzzi 21, 10129, Torino, Italy
[b] Laboratoire Réactions et Génie des Procédés, Université de Lorraine, CNRS, LRGP, F- 54000 Nancy, France
luca.marmo@polito.it

Hartmann tube equipment is used in the dust explosion experimental test to screen the flammability of powdered materials (according to ISO 80079-20) and to determine the Minimum ignition energy of dust (UNI EN 13824:2004). For the test, the nominal concentration, as the ratio between the dust sample mass and the chamber test volume (1.2 liters), is considered, assuming a uniform concentration distribution. Even though adopted as standard procedure, this approach does not consider the dust cloud's non-stationary conditions inside the tube: the effect of turbulence decrease and dust sedimentation during the test duration will affect the dust concentration locally and globally within the test enclosure. Moreover, it is well known that the turbulence intensity influences Minimum Ignition Energy.
This work derives from previous investigation on describing the dust cloud behavior within dust explosibility laboratory apparatuses. High-speed video recordings have recently been adopted to support the dust cloud dynamic analysis and visualize the cloud dispersion within a standard test setup, as the 20 L sphere and the modified Hartmann tube. This work intends to use different high-speed videos of dust dispersions in the modified Hartmann tube, with different injection pressure and sample mass, to focus on the behavior of the cloud at the typical delay time of the MIE measurement, i.e., 60-180 ms. Each video is processed frame by frame to reveal information on the cloud dynamics, otherwise hidden. The dust dynamic is accounted for calculating the variation in time of the brightness of pixels.
This way, it is possible to obtain a set of data that incorporate the effects of the dust cloud distribution and the velocity of the particles' clusters. The experimental data processing will help to focus on the time-scale and the length scale of the turbulence. The next study will focus on evaluating the time and space scale of the dust cloud and identifying the effect of ignition time delay on the MIE measurement to provide indications to operate at the most conservative conditions (higher concentration) and to avoid issues and under/overestimates due to agglomeration, sedimentation or segregation of dust particles.

1. Introduction

It is well known today that the dust cloud's fluid dynamics has fundamental importance on the cloud's behavior during the explosion. Several researchers have shown that the cloud's turbulence affects both the flame speed, and therefore the Kst, and the minimum ignition energy. It is well known that an increase in cloud turbulence determines the increase of the Kst and, at the same time, increases the MIE. Moreover, the dust concentration also significantly affects the deflagrating parameters, which are maximum near the stoichiometric concentration and decrease as the dust concentration varies towards the MEC. These considerations are relevant, whatever the parameter is intended to measure, especially regards to MIE. Current standards state that a Hartmann tube must be used to measure the MIE of dust, where the cloud is created using an air pulse obtained by discharging the air contained in a tank at a pressure of 7 bar_g into the tube.
The cloud is then subjected to an attempted ignition with an electric arc, which is triggered after a specific time (delay time): The ISO 80079 standard suggests adopting delay times between 60 and 180 ms, and it is known

that the value of MIE is influenced by the ignition delay time, as is logical since the dust cloud thus created has a distinctly transitory character, and the turbulence decreases with time. Hartmann's tube is also used to carry out the flammability screening test, which has been shown to be effective for detecting combustible dust in large sets of samples (Danzi & Marmo, 2019, Marmo & Danzi 2018, Marmo et al. 2018, 2017).
The literature contains some studies of cloud fluid dynamics in the Hartmann tube, but all focus primarily on the behavior of the very early stages of cloud formation. Murillo et al. (2013) studied the front of the cloud as it reaches the electrodes' position using high-speed films, while Hosseinzadeh et al. (2018) evaluated the flow field with PIV technology up to 120 ms. On the other hand, in the literature, there are no studies on the behavior of the cloud in the time interval suggested by the standard for carrying out the MIE measurement.
This work aims to study the behavior of the cloud in the time interval useful for measuring the MIE. For this purpose, high-speed films (2000 fps) of corn-starch clouds in Hartmann tube were made by a video camera in the visible range. The films were subsequently processed using image processing techniques to highlight the cloud's turbulent behavior and to obtain information to be compared to local concentration measurements.

2. Material and methods

2.1 Powder

Dispersion tests were performed on wheat starch provided by Sigma-Aldrich. This powder was chosen due to its numerous industrial applications and because its ignition and explosion parameters have already been widely studied by several authors (Zhang et al., 2017). Scanning electron microscopy showed that the sample is composed of ovoid to spherical particles. Particle size distribution (PSD) was measured in situ in the tube with a laser sensor (R3 lens, Helos - Sympatec). The PSD is unimodal, and d_{10}, d_{50}, and d_{90} values from the volume distribution are 28.2 µm, 65.2 µm, and 83.1 µm, respectively. The larger particles are constituted of agglomerates, which can notably be due to moisture content ranging between 8.8 and 11.5% (Sigma-Aldrich).

2.2 Dust dispersion tests

A modified Hartmann tube was used to study the dust dispersion dynamic. Such tube is used to assess if the powder is combustible or not and determine its minimum ignition energy according to ISO 80079-20-2:2016. The setup is a 1.2L cylindrical glass tube (68 mm internal diameter and 300 mm height) closed at its lower part by a dispersion cup equipped with a mushroom-shaped nozzle. The powder is placed in the cup and is then dispersed by an air blast along the vertical tube. Even if no ignition was performed during these tests, two electrodes were placed at 100 mm from the bottom of the tube but were not electrically connected.
According to ISO 80079-20-2:2016, the air pressure is set at 7 bar_g to generate a ‘uniformly dispersed’ dust cloud at 1 atm. Obviously, it appears that both the volume (thus the local concentration) and the homogeneity of the dust cloud vary significantly as a function of the density, size, and shape of the powders. Therefore, the influence of the overpressure was studied, and two dispersion procedures were applied. For tests at 7 barg, the standard procedure was used using the Mike 3 software provided by Kühner AG. As the latter does not allow to work at low air pressures, tests at 3.5 bar_g were carried out using an external 50 mL cylindrical tank, equipped with two electrovalves and a manometer, and connected to the dispersion cup.
The dust dispersion was recorded during approximately 500 ms, using a high-speed video camera (MotionBlitz EoSens mini2) at 2000 fps. In order to limit interfering reflections, Mike 3 door was removed, a black screen was placed in the background, and a halogen lamp was used as additional light.

3. Post-processing operations

An elaboration software for the high-framerate videos was written in LabVIEW®. The aim was to subtract the background luminance, thus keeping the video information due to the clouds only, and possibly step from the usual frame sequence to a set of differential calculation schemes.
The data elaboration and collection consist of three subsequent stages:

- preliminary video filtering
- row luminance detection
- luminance data presentation and recording

3.1 Preliminary video filtering

The differential video signal was introduced to enhance the regions in which the cloud’s movements happen, thus giving precious information on the cloud dynamics. This first elaboration step that also includes an option for background cancellation is summarized as Video Filtering.
The program allows the selection of several filtering modes to cancel the fixed background image data, leaving the dust cloud-only representation.

The canceling methods mainly consist of two different and alternative processes, each one leading to specific benefits and drawbacks. Each pixel will undergo the following actions:

- the subtraction of the data of the first frame throughout the whole video also named *InitialDifference* or $\sum_{i=1}^{N}(n_i - n_0)$;
- the subtraction of a previous frame from the actual frame image data, also named *DeltaFrame* or $\sum_{i=1}^{N}(n_{i+x} - n_i)$.

The *InitialDifference* is properly a background luminance subtraction: it produces clear, non-differential images of the cloud. The drawback is the generation of dark spots and artifacts in the areas where the background is brighter. Every single bright object in the background, or even a reflection of the test lights on the tube, can produce an unwanted cloud data cancellation. This calculation mode is requiring careful use of light and proper background objects masking.

The *DeltaFrame* mode shows different behavior, being less sensitive to the background data. The resulting video shows brighter only the areas in which the luminance varied from the x previous frame. The luminance can be higher or lower than in the previous frame. Two revelation modes are available:

- ✓ absolute value mode, in which both the positive and negative luminance variation causes a luminance increment;
- ✓ positive-only mode, in which the negative portion does not produce a signal, and the bright areas strictly represent a raise in luminance.

The second, positive-only mode ($\sum_{i=1}^{N}(n_{i+x} - n_i)\,, only\ (n_{i+x} - n_i) > 0$) leads to the best results due to the absence of the duplication effect: in the absolute mode, a single particle or aggregate moving sufficiently fast displays twice, both in its new and in its old position.

A useful variation of the *DeltaFrame* mode was obtained by performing the subtraction on non-consequential frames by subtracting the second last frame from the actual frame (or the third last or fourth last, and so on). So, a *DeltaFrame* numerical parameter is defined that specifies the number of frames to be skipped, from 1 to 20. Depending on the number of skipped frames, different information on the cloud's mass displacement is revealed. It will be referred to as *"DeltaX"* hereon. The video framerate is 2000 fps. The video color depth is 8 bit (grayscale), so the unsigned, 8-bit grayscale format is used in the software. The internal calculations are performed in the unsigned 16-bit grayscale format or in double precision floating point format and then converted back to 8-bit grayscale for graphical representation.

Thus, a filtered video is obtained and saved (both as a whole and as an image set) having the same framerate and frame count as the original one.

3.2 Row luminance detection

A second elaboration is then performed on the filtered video.

All the luminance values of the pixels in the same row, corresponding to a specific height on the tube, are taken together and fed to a detecting stage, which is available in three different modes:

- maximum value detector: returns the maximum luminance level on the row;
- standard deviation: returns the standard deviation of the luminance of the row's pixels;
- average value: computes the average luminance level of the row.

Each row's luminance data are then collected and presented in two graphical ways: an evolving, single-waveform graph showing the luminance curve versus height and an intensity chart in which the luminance versus height history is recorded.

4. Results and discussions

The post-treatment of the images proposed in section 3 allows highlighting the variations in the concentration of the powder and, consequently, highlighting the cloud's fluid dynamics structure.

Figure 1 compares the original image and the post-processed image. It is evident that the second contains a greater quantity of information: in particular, the areas where there are variations in brightness (therefore in dust concentration) are highlighted. Clusters of homogeneous concentration attributable to eddies are also clearly visible and contain information on the turbulence's intensity. On the other hand, the original image is affected by background objects that may confuse the reader. Also, the cloud front is very evident in the processed image, while it is hard to find in the original one. The analysis of the processed movie will allow following the cloud front strictly. Velocity measurements of the dust front will also take advantage of post-treatment (not shown in this paper).

In the following figures 2 to 4, the original images at different times and test conditions are proposed together with the processed images. The latter differ in the delta frame applied in post-processing (x=1, 5, 20) for systematic comparison. The runs are made using 300 mg of corn starch; the air pulse pressure is 7 bar.

It is evident that the processed images' information depends on the delta frame used and the local speed of the dust cloud. Figure 2 refers to the initial phase of cloud formation (t = 0.04s) when the cloud's speed is high, and turbulence is very intense. In this phase, the *Delta1* image clearly describes the structure of the concentration field. On the contrary, the *Delta5* and *Delta20* images progressively lose information and appear as "blurry". This effect probably depends on the fact that, given the high speed, the eddies travel a great distance along with x frames and change shape during the shooting of 20 or even only 5 frames, so they are no longer recognizable when X grows.

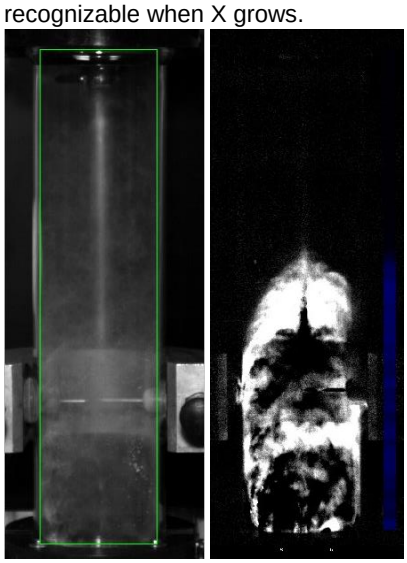

Figure 1: Original and post-processed image

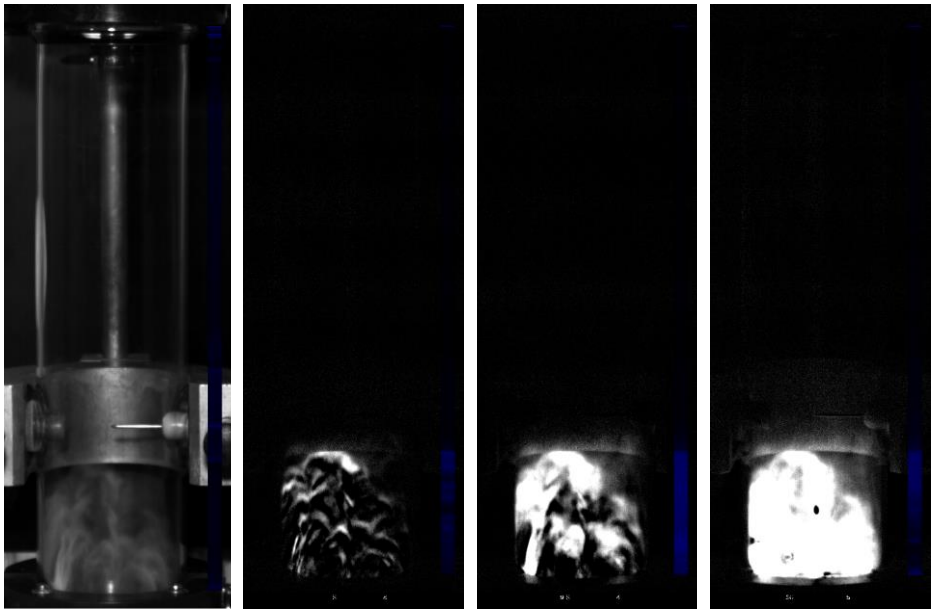

Figure 2: Original and post-processed image, Delta1, 5, and 20, respectively. The image was taken at 0.04 s.

On the contrary, when we consider the images taken after 0.1 s (when the flow has reduced his speed to a moderate value), the best choice seems to be *Delta 5* (Figure 3). Note that the cloud does not appear to occupy the whole Hartmann tube at this stage. As expected, the turbulence scale has significantly decreased with respect to 0.04s (Figure 2). Finally, the images taken at 0.25 seconds, when the cloud is practically in free fall, are optimally processed by delta 20. Here the turbulence scale has further decreased. The eddies are barely visible, likely because the dust concentration is almost homogeneous.
In addition to the concentration clusters, some aggregates of particles almost not visible in the original image are instead evident. It is still unclear whether these lumps are present at the earlier stage of the cloud life, or

instead, they form during the particle motion. These lumps may indicate that the dust dispersion process is not efficient at the experimental condition used, which are those suggested by UNI EN 13824:2004 for MIE measurement.
It is worth noting that the dust concentration at the electrodes' location and turbulence is unsteady in the time interval suggested for MIE measurements. Ongoing experiments with different dust and mixtures will help clarify the dust characteristics' effect on the cloud behavior in the interval 0-300 ms, which was already demonstrated evident in the 20l sphere (Di Sarli et al. 2019).

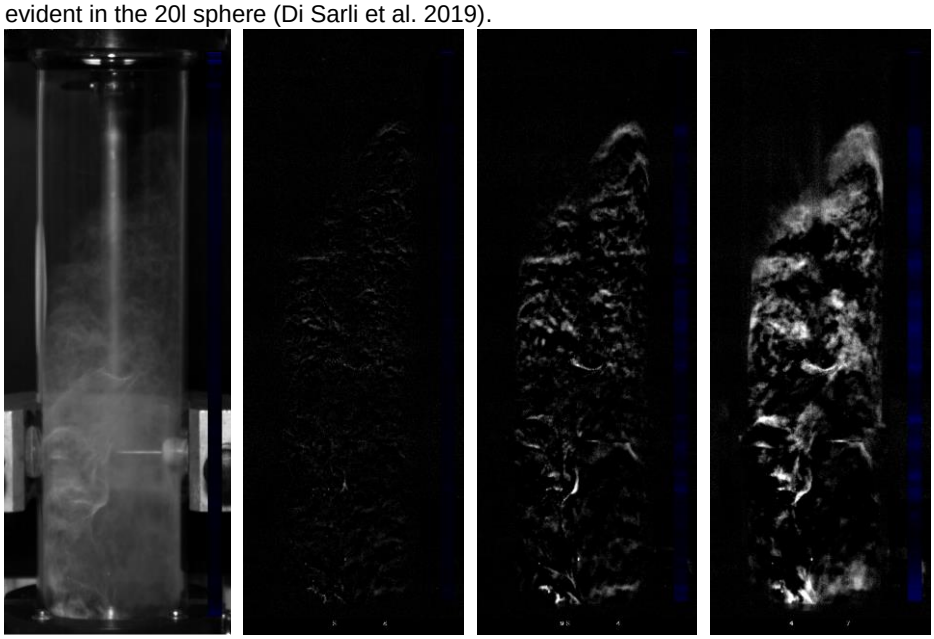

Figure 3: Original and post-processed image, Delta1, 5, and 20, respectively. The image was taken at 0.1 s

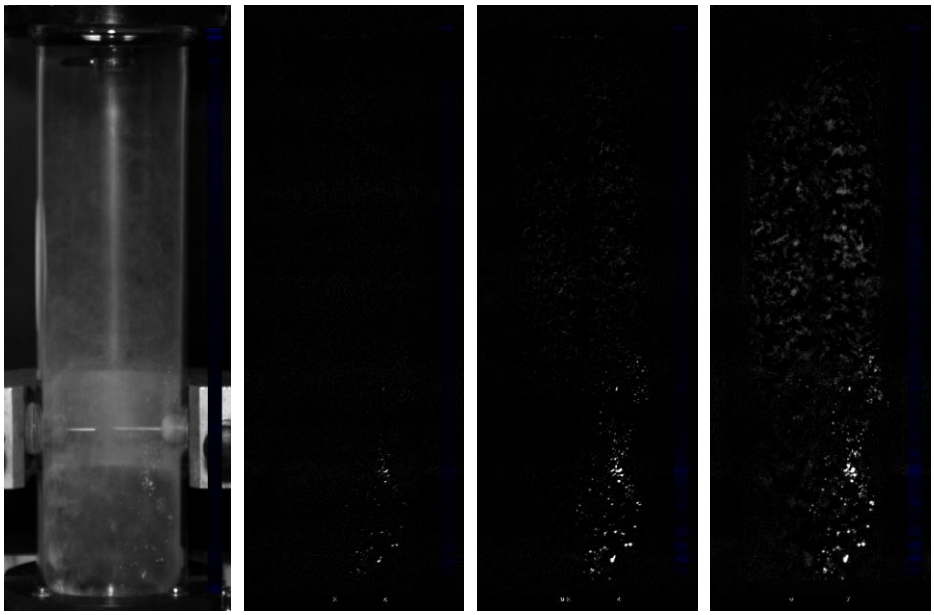

Figure 4: Original and post-processed image, Delta1, 5, and 20, respectively. The image was taken at 0.25 s

Figure 5 shows the processed image (up left), the evolving, single-waveform graph showing the luminance curve versus height (bottom left), and the intensity chart in which the luminance versus height history is recorded (right).
The latter representation allows following the cloud's propagation along the tube. By setting the proper luminance threshold and by detecting the front of the cloud, the propagation speed may be measured accurately.

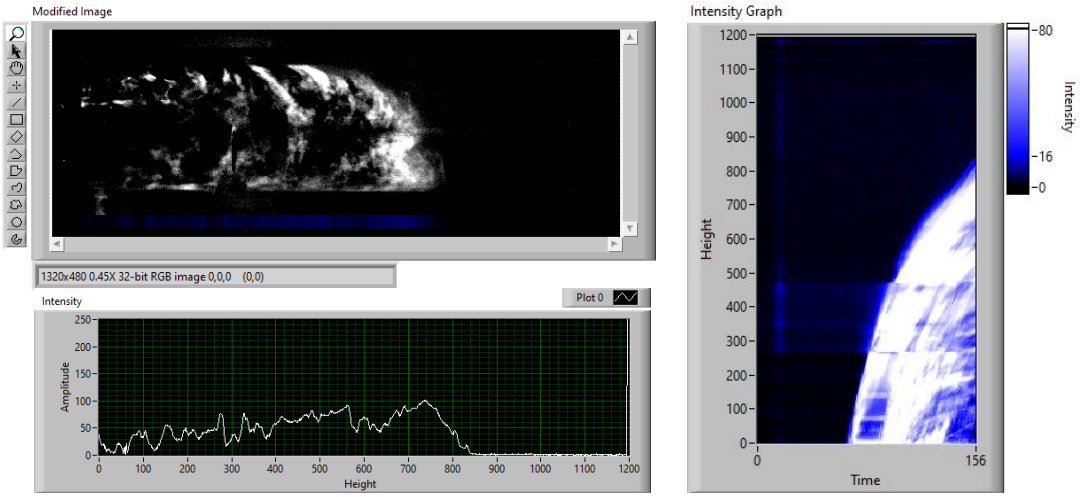

Figure 5: Visualisation of the LabVIEW® front panel: (clockwise direction) modified image; luminance versus height history intensity chart; single waveform luminance vs. height graph.

5. Conclusions

Images extracted from high-speed (2000 fps) footage of Hartmann's tube dust clouds were post-processed using the *DeltaFrame* method, using different deltas. The images thus obtained are rich in information about the change in properties of the cloud, which can be used to extract information relating to the turbulence scale and the solid's local velocity. The standard deviation of the intensity will be correlated to the time and length scale of turbulence to this aim. The information obtained depends on the delta used. The optimal delta seems to depend on the speed of the solid. This work has to be regarded as a preliminary approach to the investigation of dust cloud dynamics within the Hartman tube through high-speed video post-processing and, with further verification tests (different operative conditions and/or type of dust), could constitute a relatively quick procedure to study turbulence structures and the adequate time scale to operate the MIE test. Furthermore, the same procedure will be applied to ignition tests to correlate turbulence intensity in the flow to flame development and propagation.

References

ASTM E2019 - 03(2019) Standard Test Method for Minimum Ignition Energy of a Dust Cloud in Air

Danzi, E., Marmo, L. (2019), Dust explosion risk in metal workings Journal of Loss Prevention in the Process Industries, 2019, 61, pp. 195–205. 10.1016/j.jlp.2019.06.005

Di Sarli, V., Danzi, E., Marmo, L., Sanchirico, R., Benedetto, A.D. (2019), Issues of “Standard” explosion tests for non-spherical dusts Chemical Engineering Transactions, 77, pp. 691–696. 10.3303/CET1977116

Hosseinzadeh, S., Vanierschot, M., Norman, F., Verplaetsen, F., Berghmans, J. (2018). Flame propagation and flow field measurements in a Hartmann dust explosion tube. Powder Technology, 323, 346–356. 10.1016/J.POWTEC.2017.10.001

ISO /IEC 80079-20-2:2016 Explosive atmospheres - Part 2 0-2: Material characteristics - Combustible dusts test methods

Marmo, L., Danzi, E. (2018), Metal waste dusts from mechanical workings - explosibility parameters investigation, Chemical Engineering Transactions, 67, pp. 205–210. 10.3303/CET1867035

Marmo, L., Sanchirico, R., Di Benedetto, A., Di Sarli, V., Riccio, D., Danzi, E. (2018), Study of the explosible properties of textile dusts Journal of Loss Prevention in the Process Industries, 54, pp. 110–122. 10.1016/j.jlp.2018.03.003

Marmo, L., Riccio, D., Danzi, E. (2017), Explosibility of metallic waste dusts Process Safety and Environmental Protection, 2017, 107, pp. 69–80, 10.1016/j.psep.2017.01.011

Murillo, C., Dufaud, O., Bardin-Monnier, N., López, O., Munoz, F., & Perrin, L. (2013). Dust explosions: CFD modeling as a tool to characterize the relevant parameters of the dust dispersion. Chemical Engineering Science, 104, 103–116. 10.1016/J.CES.2013.07.029

Zhang, H., Chen, X., Zhang, Y., Niu, Y., Yuan, B., Dai, H., He, S. Effects of particle size on flame structures through corn starch dust explosions (2017) Journal of Loss Prevention in the Process Industries, 50, pp. 7-14. 10.1016/j.jlp.2017.09.002